



## Influence of control parameters on the crack paths in the aluminum alloy 2024 under bending

E. Marcisz, D. Rozumek, Z. Marciniak

*Opole University of Technology, Poland*

*marciszewa@wp.pl, d.rozumek@po.opole.pl, z.marciniak@po.opole.pl*

**ABSTRACT.** The paper presents development of crack paths in aluminium alloy 2024. Fatigue tests were carried out for specimens with rectangular cross-section. The specimens were put to bending at controlled energy parameter amplitude and bending moment amplitude. The proposed method of conducting research with the controlled energy parameter has been presented in [1]. The energy parameter model proposed by Macha has been used in the tests. Tests with controlled energy parameter amplitude allow observing crack growth depending on maximum shearing stress surface. Tests with controlled bending moment amplitude allowed observing two types of crack paths.

**KEYWORDS.** Energy parameter; Bending moment; Crack growth.

### INTRODUCTION

In majority, engineering structures, machines and technical devices struggle against material fatigue problem. Literature sources broadly specify the methods for fatigue life assessment and diagnosing the reasons of damage. Material fatigue life is described using fatigue characteristics: stress ( $\sigma_a-N_f$ ), strain ( $\epsilon_a-N_f$ ) and energy ( $W_a-N_f$ ). Most frequently, fatigue test results are illustrated by Wöhler fatigue characteristic. Manson–Cofin–Basquin formulas describe material fatigue life using strain characteristics. Specification of stress and strain characteristics is defined in the ASTM standard [2, 3]. Whereas, fatigue characteristics obtained during tests with energy parameter control were proposed in the studies [1, 4]. Observations and analyses of crack path development are carried out in order to obtain additional information concerning changes occurring in a material.

Different fatigue crack paths are observed during tests, depending on material used and loading type. Growth rate of these paths has direct effect on material life.

The aim of the paper is comparison of crack paths in aluminum alloy 2024 for bending tests performed with controlled energy parameter amplitude and bending moment amplitude.

### THE MATERIAL AND TEST PROCEDURE

The material tested is aluminium alloy 2024, characterised by low resistance to oxidation, non-weldability and average workability. This material is used to make shafts, screws, pistons, couplings, hydraulic valves and aircraft parts. Tab. 1 shows chemical composition of the material and Tab. 2 specifies static properties of aluminium alloy 2024.



Cu	Mn	Zn	Mg	Fe	Cr	Si	Ti	Al
4.40	0.62	0.08	1.70	0.25	0.01	0.13	0.05	Balance

Table 1: Chemical composition (in wt %) of the 2024 aluminium alloy

$\sigma_y$ (MPa)	$\sigma_u$ (MPa)	E (GPa)	A <sub>5</sub> (%)
432	552	77.5	12

Table 2: Mechanical properties of the 2024 aluminium alloy

Aluminium alloys containing copper and magnesium, that is duralumin, are among materials characterised by high strength properties. In the structure of a specimen cut off along the rod axis, are visible elongated grains of the  $\alpha$  solid solution as well as numerous precipitations of the intermetallic phase  $\text{CuAl}_2$ ,  $\text{Al}_3\text{Mg}_2$ ,  $\text{Al}_6\text{Mn}$  containing iron  $\text{Cu}_2\text{FeAl}$  arranged in a streaked way, mainly on the grain boundaries (Fig. 1). Precipitations of these phases significantly influence on strength and hardness of 2024 aluminium alloy. In particular, the precipitations in the phase boundaries decrease the plastic properties.

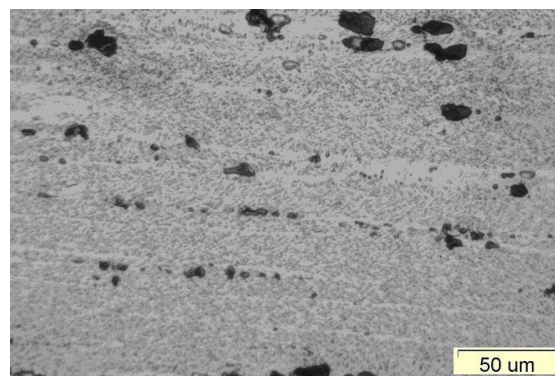


Figure 1: The 2024 aluminium alloy microstructure under magnification 500x

Test pieces are square cross-section specimens taken from a bar 20 mm in diameter, shown in Fig. 2.

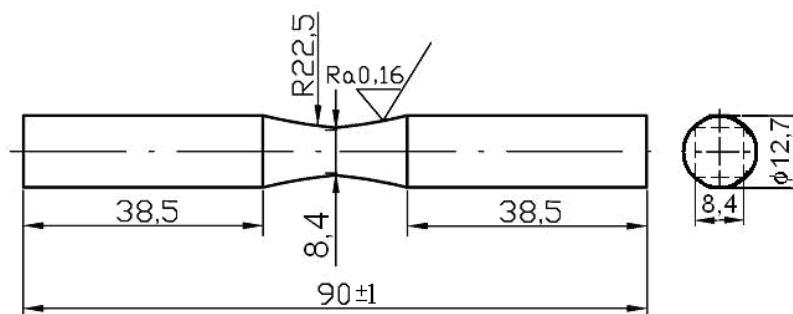


Figure 2: Shape and dimensions of specimen (in mm).

The specimens have been tested on MZGS-100Ph fatigue test stand, shown in Fig. 3. The test stand enables conducting structural material test, subjected to bending, torsion or various combinations of sine bending-torsional loads. The test stand is composed of three sub-assemblies: the loading one, the driving one and the control and measurement one. The driving sub-assembly transmits its rotational speed from motor through the driving belt transmissions to the loading sub-assembly. The loading sub-assembly consists of vibrators loaded with weights, rods, levers and springs. Unbalanced



rotation motion of vibrators generate vertical moves of lever which caused loading of specimens. The control and measuring sub-assembly records histories of stresses, strains, energy parameter and hysteresis loops [5].

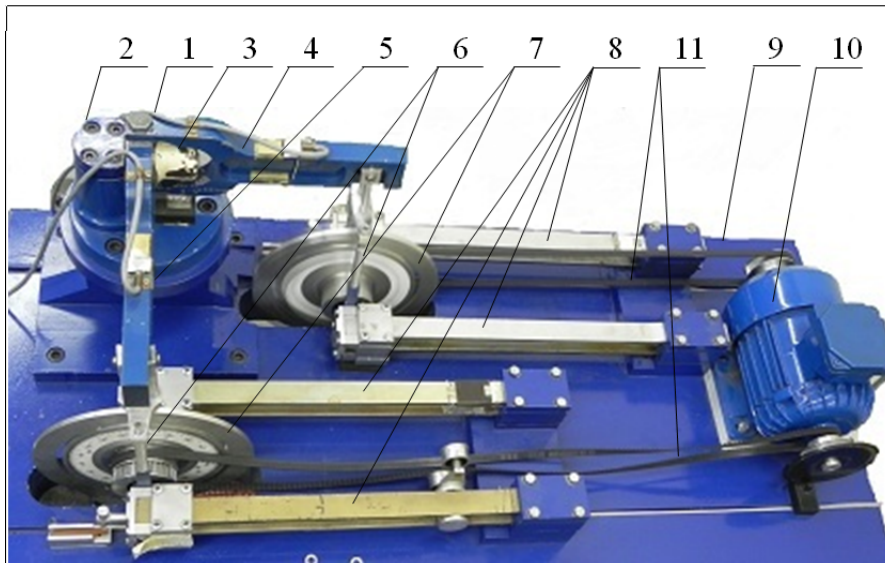


Figure 3: Fatigue test stand MZGS-100Ph: 1 – specimen, 2 – clamp, 3 – grip, 4 – bending lever, 5 – rod, 6 – vibrator discs, 7 – springs, 8 – flat springs, 9 – machine base, 10 – engine, 11 – toothed belts.

In the closed-loop control system of test stand MZGS-100Ph the amplitude  $W_a$  of a new energy parameter for determination of fatigue characteristic under cyclic bending was used. The history of normal strain energy density parameter  $W(t)$  is defined as [6]

$$W(t) = 0,5\sigma(t_i) \cdot |\varepsilon(t_i) - \varepsilon_i^{pl}| \quad (1)$$

where  $\varepsilon_i^{pl} = \varepsilon(t_i)$  for  $\sigma(t_i) = 0$  and  $i = 1, 2, 3, \dots$

In Eq. (1)  $\varepsilon_i^{pl}$  is the plastic strain registered in the moment  $t_i$ , when the stress  $\sigma(t_i)$  is equal to zero, and remains constant to the moment  $t_{i+1}$  when the stress reaches zero again, i.e.  $\sigma(t_{i+1}) = 0$ . Then the new registered value of plastic strain  $\varepsilon_{i+1}^{pl}$  replaces the previous one  $\varepsilon_i^{pl}$ . This procedure is repeated for each cycle of bending.

A sample trajectory of energy parameter is shown in Fig. 4. Fig. 4a presents energy parameter course according to the Smith-Watson-Topper relationship [7], and Fig. 4b the course of modified energy parameter. Fig. 4 allows observing that parameter  $W_{aSWT}$  applies to positive values only, while the parameter defined by formula (1) applies both to positive and negative values.

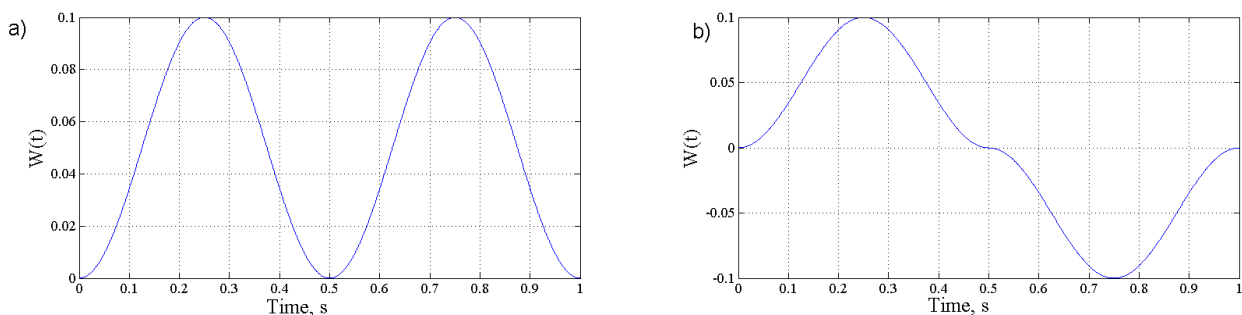


Figure 4: Comparison of energy parameter courses: a) according to Smith-Watson-Topper relationship, b) according to modified energy parameter.



## TEST RESULTS

The 2024 aluminum alloy specimens were tested under bending with range frequency of 11-14 Hz and a given amplitude parameter in the range of  $W_a = 0.2-0.4$  MJ/m<sup>3</sup>. During the tests, histories of stress, strains, energy parameters and hysteresis loops, ( $\sigma$ - $\epsilon$ ), were measured and registered. Fatigue test with controlled bending moment amplitude have been conducted in range  $\sigma_a = 187.5 - 255$  MPa.

Fig. 5 shows the exemplary history of energy parameter,  $W(t)$ , and in Fig. 6 the history of stresses,  $\sigma(t)$ , and strains,  $\epsilon(t)$ , (the first 6 blocks cover from 0 to 64000 cycles, the next 2 blocks represent cycles from 64000 to 166000 cycles). The example, shown in Fig. 5 concerns the results of the amplitude of the energy parameter  $W_a = 0.30$  MJ/m<sup>3</sup>, the specimen, which was failed after  $N_f = 348100$  cycles. Based on the present course of  $W(t)$ , it can be seen slight fluctuations in the amplitude  $W_a$ , which are the result of periodic (non-continuous) calculations of this amplitude in the control system for the new values of stresses and strains. Relative error,  $\Delta W$ , in this example was below 10%.

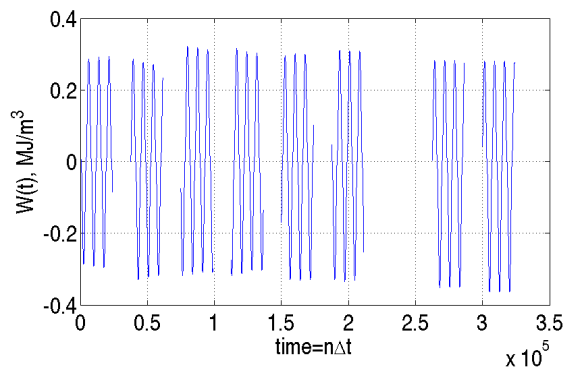


Figure 5: Exemplary history of the energy parameter,  $W(t)$ , under bending in the function of time,  $t = n\Delta t$ ,  $n$  - number of discrete history values,  $\Delta t = 1.2987 \cdot 10^{-5}$  s - sampling time

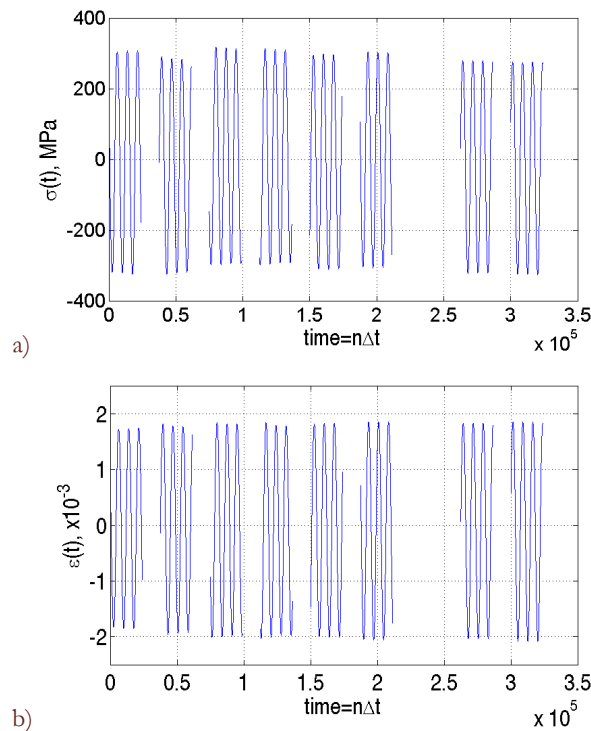


Figure 6: An exemplary history: a) - the stress  $\sigma(t)$ , b) - strain  $\epsilon(t)$  under bending in the function of time,  $t = n\Delta t$ ,  $n$  - number of discrete history values,  $\Delta t = 1.2987 \cdot 10^{-5}$  s - sampling time



From the diagrams in Fig. 6, it can be observed that the values of stresses and strains in registered histories slightly oscillate around some fixed values. A small decrease of stress can be observed at the initial stage of test (Fig. 6a), whereas strain presents the opposite behaviour (Fig. 6b). Thereafter, both histories stabilize during the test.

Fig. 7 presents 2024 aluminum alloy fatigue characteristics, determined on the base of tests with controlled energy parameter amplitude  $W_a$  at bending. The tests have been performed at four levels  $W_a = 0.2, 0.3, 0.35, 0.4$  MJ/m<sup>3</sup>.

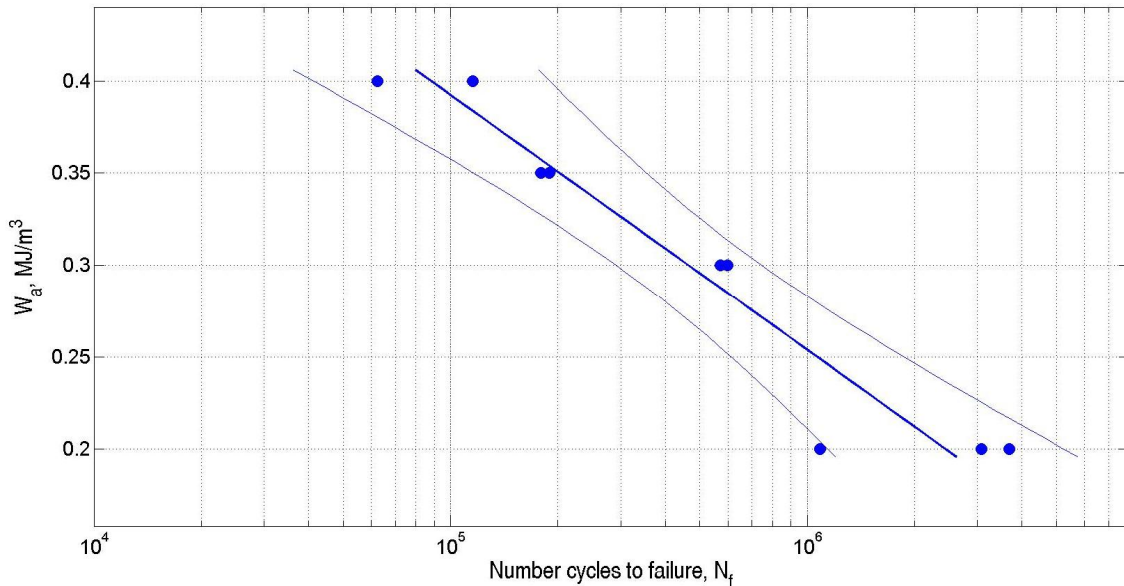


Figure 7: The fatigue characteristic ( $W_a$ - $N_f$ ) of 2024 aluminum alloy under bending with a controlled amplitude of the energy parameter.

Fig. 8 presents 2024 aluminum alloy fatigue characteristics, determined with controlled amplitude of the bending moment  $\sigma_a$  at bending. In the range of finite lifetime, the tests have been executed at five levels  $\sigma_a = 187.5, 200, 232, 233, 255$  MPa. At least two specimens were tested at each of stress levels.

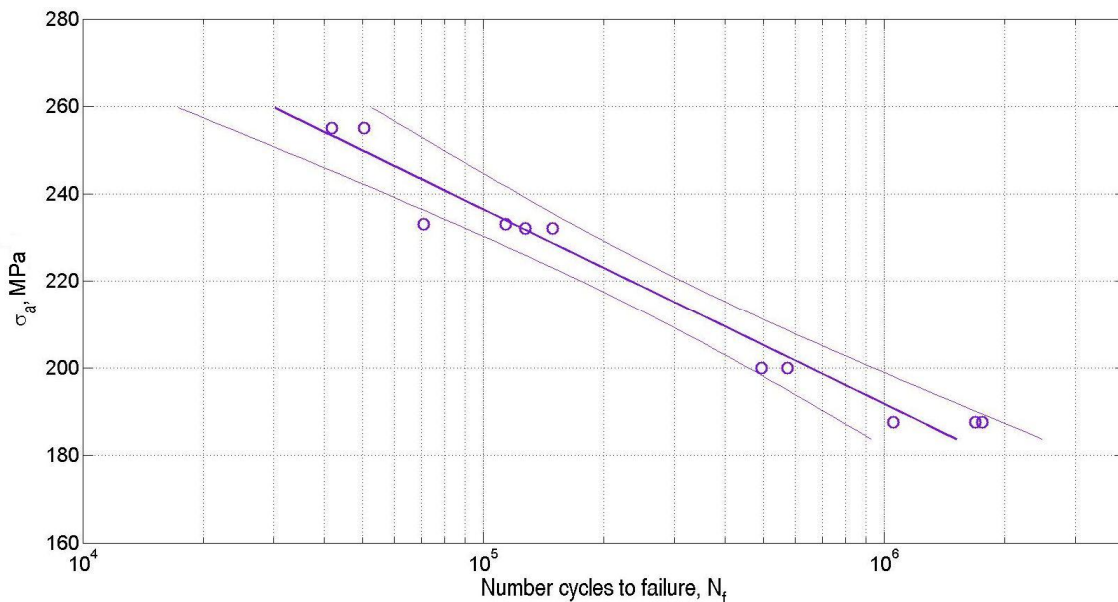


Figure 8: The fatigue characteristic ( $\sigma_a$ - $N_f$ ) of 2024 aluminum alloy with controlled amplitude of the bending moment

Fig. 9 presents fatigue characteristic of 2024 aluminum alloy with controlled amplitude of the bending moment  $\sigma_a$  and energy parameter  $W_a$ . Knowing the values obtained during tests at controlled amplitude of the bending moment  $\sigma_a =$



187.5, 232, 233, 255 MPa, values of elastic energy have been calculated according to linear-elastic model of solid ( $W_a = \sigma_a^2/2E$ ), obtaining  $W_a = 0.23, 0.28, 0.34, 0.36, 0.42$  MJ/m<sup>3</sup>.

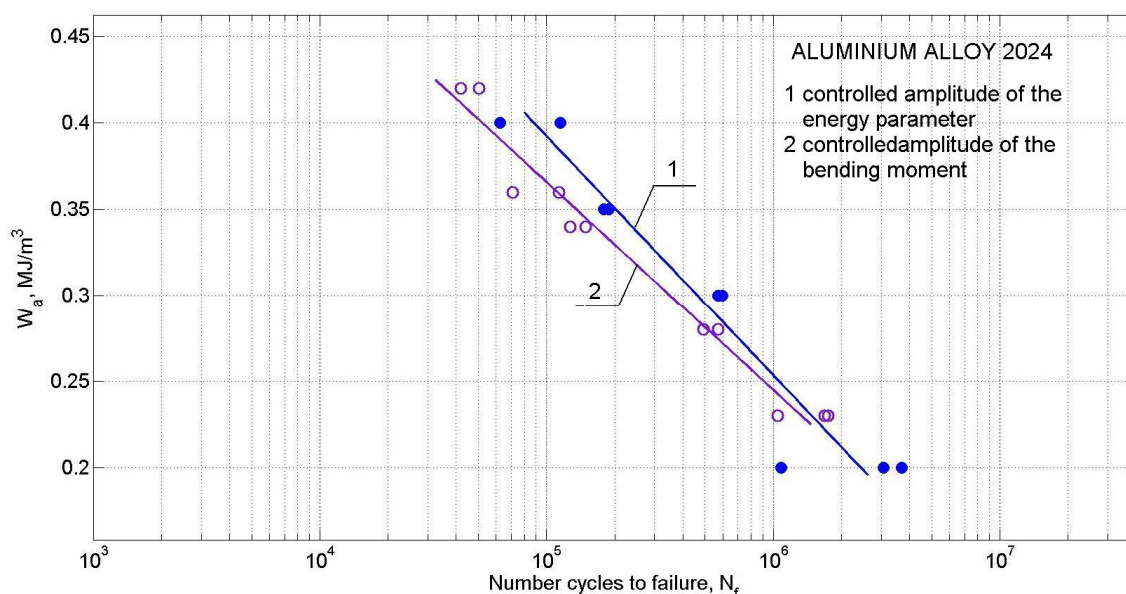


Figure 9: The fatigue characteristic of 2024 aluminum alloy under bending with a controlled amplitude of the 1 – energy parameter with Eq. (1), 2 – energy parameter with linear-elastic model of solid.

The results of fatigue tests have been subjected to statistical analysis, and calculated according to relations (2) and (3), coefficients of regression equation and correlation are shown in Tab. 3.

$$\log N_f = A + m \cdot W_a \tag{2}$$

$$\log N_f = A + m \cdot \sigma_a \tag{3}$$

where:

$W_a$  - amplitude of energy parameter,

$\sigma_a$  - amplitude of nominal stress,

$N_f$  - number of cycles to failure,

$A$  i  $m$  - coefficients of the regression equation

Material	A	B	r	Type of research
2024	7.030	-7.216	0.960	Controlled energy parameter amplitude - Eq. (2)
2024	10.293	-0.022	0.981	Controlled bending moment amplitude - Eq. (3)

Table 3: Coefficients of the regression equation and correlation at a significance level,  $\alpha = 0.05$  with a controlled amplitude of the nominal stress.

Cracks of specimens from aluminium with  $\alpha$  phase structure occur in the slip plane  $\{111\}$  under shear stress, which are almost independent of grains space orientation. In the specimen (Fig. 10) it is observed the main, zigzag crack developed through transcrystalline  $\alpha$  phase grains. This crack is changing direction on grain boundaries. It can also be noticed some side, short cracks running in parallel to the main crack. The characteristic feature of the main crack are slips occurring under angle  $45^\circ$  to specimen axis.



Figure 10: Fatigue crack path of the aluminium alloy 2024.

A sample development of crack paths at controlled energy parameter is shown in Fig. 11. Fig. 11a presents crack path observed at energy parameter  $W_a = 0.4 \text{ MJ/m}^3$ ; the specimen was damaged after 11550 cycles. Fig. 11b shows crack path for a specimen examined at energy parameter value  $W_a = 0.35 \text{ MJ/m}^3$ ; the specimen was damaged after 88900 cycles. A sample development of crack paths under bending moment control is illustrated in Fig. 12. Crack path in Fig. 12a was observed at stress value  $\sigma_a = 255 \text{ MPa}$ , which according to linear-elastic model corresponds to energy parameter  $W_a = 0.42 \text{ MJ/m}^3$ ; the specimen was damaged after 50300 cycles. Fig. 12b shows crack path obtained during tests for stress  $\sigma_a = 233 \text{ MPa}$ . According to linear-elastic model, it corresponds to energy parameter  $W_a = 0.36 \text{ MJ/m}^3$ . The specimen was damaged after 70800 cycles. Presented photos allow observing that crack paths in Figs. 11a and 12a develop in much the same way. Greatest changes in crack path development directions (zigzag) were observed during tests at controlled bending moment amplitude  $\sigma_a = 233 \text{ MPa}$  (Fig. 12.b). In case of controlled energy parameter and bending moment the specimens had different cracking courses. After initiation, cracks develop along different planes, where the plane of highest shearing stress is prevailing.

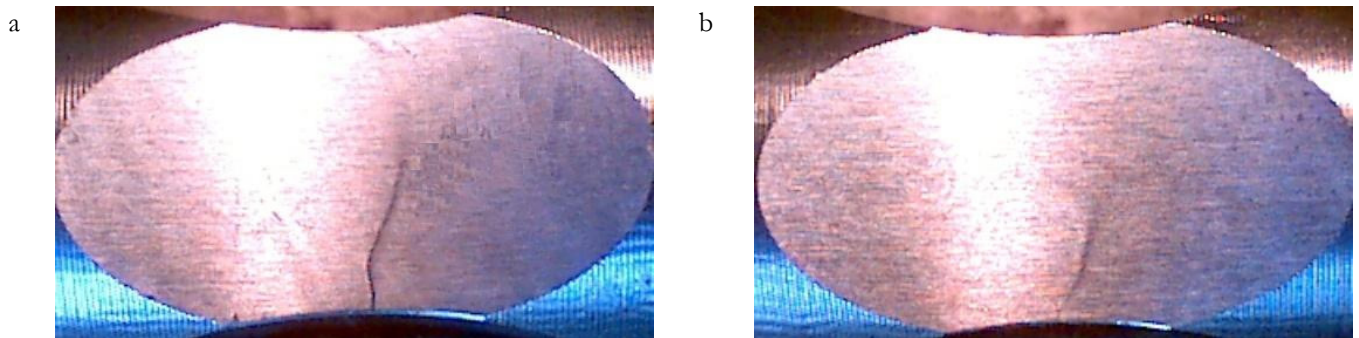


Figure 11: Fatigue crack path for controlled amplitude of the energy parameter

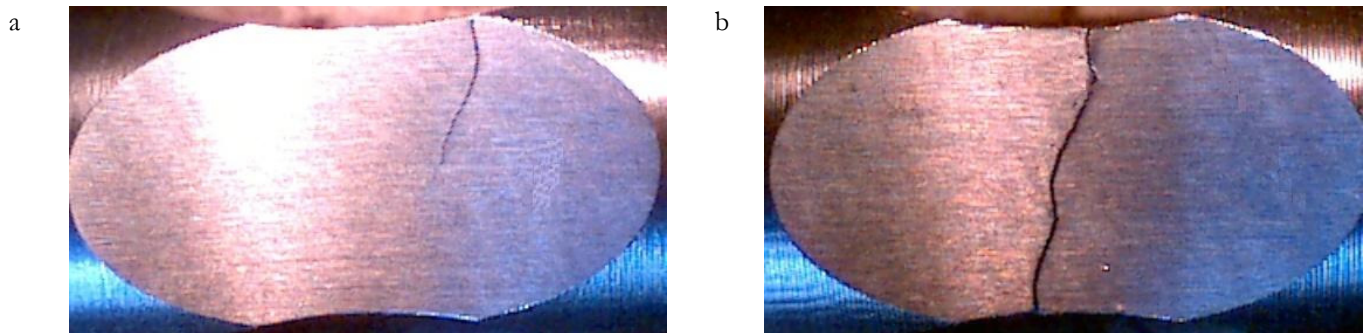


Figure 12: Fatigue crack path for controlled amplitude of the bending moment.



## CONCLUSIONS

The following conclusions were formulated on the basis of alloy 2024 tests carried out with controlled energy parameter amplitude and bending moment amplitude:

1. Life of specimens at controlled energy parameter is slightly better than life of specimens at controlled bending moment amplitude.
2. The characteristics show converging tendency at lower values of the parameters, which is the effect of strains being taken into consideration (or not).
3. Depending on applied load and parameter, fatigue crack paths had different courses.

## REFERENCES

- [1] Marcisz, E., Marciniak, Z., Rozumek, D., Macha E., Fatigue characteristics of aluminium alloy 2024 under cyclic bending with the controlled energy parameter. *Key Engineering Materials*, 592-593 (2014) 684-687.
- [2] ASTM E 606-80. Standard practice for: Statistical analysis of linearized stress- life (S-N) and strain-life ( $\epsilon$ -N) fatigue data [in:] *Annual Book of ASTM Standards*, 03.01 Philadelphia (1989) 601-611.
- [3] ASTM E 739-80. Standard practice for: Statistical analysis of linearized stress- life (S-N) and strain-life ( $\epsilon$ -N) fatigue data [in:] *Annual Book of ASTM Standards*, 03.01 Philadelphia (1989) 667-673.
- [4] Marcisz, E., Marciniak, Z., Rozumek, D., Macha, E., Energy fatigue characteristic of C45 steel subjected to cyclic bending, *Key Engineering Materials*, 298 (2014) 147-152.
- [5] Achtelik, H., Marciniak, Z., Macha, E., Marcisz, E., Rozumek, D., The stand for fatigue tests of materials with the controlled energy parameter under bending and torsion, *Przegląd Mechaniczny*, Warszawa, 12 (2013) 34-38, in Polish.
- [6] Macha, E., Słowik, J., Pawliczek, R., Energy based characterization of fatigue behavior of cyclically unstable materials, *Solid State Phenomena*, 147-149 (2009) 512-517.
- [7] Smith, K., Watson, P., Topper, T., A stress-strain function for the fatigue of metals, *J. Materials*, 5 (1970) 767-779.